

Numerical Modeling of Mid-IR Lasers Based on Tb-Doped Chalcogenide Multicore Fibers

Nikolay I. Salnikov^{1,2}, Alexey V. Andrianov¹ and Elena A. Anashkina^{1,*}

¹ A.V. Gaponov-Grekhov Institute of Applied Physics of the Russian Academy of Sciences, 46 Ulyanov Street, Nizhny Novgorod 603950, Russia; n.salnikov@ipfran.ru (N.I.S.)

² Advanced School of General and Applied Physics, Lobachevsky State University of Nizhny Novgorod, 23 Gagarin Ave., Nizhny Novgorod 603022, Russia

* Correspondence: elena.anashkina@ipfran.ru

Abstract: Mid-IR fiber lasers operating at wavelengths near 5 μm are of great interest for many fundamental and industrial applications, but only a few experimental samples based on active chalcogenide fibers have been demonstrated so far. One of the limitations of the power of such lasers may be a fairly low fiber damage threshold. To solve this problem, we developed and numerically investigated in detail a mid-IR fiber laser at 5.3 μm with multi-W output power pumped into the cladding at a wavelength of 2 μm . We proposed using a Tb-doped chalcogenide multicore fiber with 25 single-mode cores arranged in a 5×5 square lattice as an active medium. The proposed laser design surpasses the power limit of single-core chalcogenide fibers. When simulating lasers, we specified realistic parameters of Tb-doped chalcogenide glass based on published experimental data. We performed a comprehensive theoretical analysis, studied the influence of various factors on the characteristics of generation, and found optimal system parameters and expected generation parameters.

Keywords: Tb-doped chalcogenide fiber; multicore fiber; mid-IR fiber laser



Citation: Salnikov, N.I.; Andrianov, A.V.; Anashkina, E.A. Numerical Modeling of Mid-IR Lasers Based on Tb-Doped Chalcogenide Multicore Fibers. *Fibers* **2024**, *12*, 25.

<https://doi.org/10.3390/fib12030025>

Academic Editor: Paulo Caldas

Received: 12 December 2023

Revised: 27 February 2024

Accepted: 8 March 2024

Published: 11 March 2024



Copyright: © 2024 by the authors. Licensee MDPI, Basel, Switzerland. This article is an open access article distributed under the terms and conditions of the Creative Commons Attribution (CC BY) license (<https://creativecommons.org/licenses/by/4.0/>).

1. Introduction

Mid-IR lasers in the 3–6 μm range are in demand for a lot of applications, including scientific, industrial, and medical ones [1,2]. However, the development of lasers in this spectral range is associated with a number of difficulties, so, today, such sources are not widespread, especially with powers at the level of several watts and above. However, significant experimental success has been achieved in this direction [2], for example, quantum cascade lasers [3–5].

Another promising way to develop coherent mid-IR sources is based on fiber lasers. These could be, for example, gas-filled hollow fiber lasers [6–9]. Hollow light waveguides of various designs are made of silica glass [10]. Even very high losses of silica glass in the mid-IR range are not a limitation because the mode is localized away from the walls of the silica waveguide. However, if we speak about lasers based on solid fibers, silica fibers are fundamentally not suitable; fibers based on soft glasses are used in these cases [1,11]. Currently, continuous-wave lasers based on fluoride fibers doped with rare-earth ions make it possible to obtain powers of tens of watts in the wavelength range of about 3 μm [12,13]. However, an advance to notably longer wavelengths in fluoride fiber lasers proves to be very difficult. The longest wavelength achieved in lasers based on fluoride fibers is 3.92 μm [14]; further increase in laser wavelength is limited by multiphonon luminescence quenching in active rare-earth ion transitions. A possible way to overcome this problem is to use chalcogenide fibers doped with rare-earth ions, in which the phonon energy is significantly lower than in fluoride fibers. Chalcogenide fibers based on glasses with various compositions doped with Tb^{3+} , Pr^{3+} , Dy^{3+} , and other ions were produced, and their optical and physicochemical characteristics were comprehensively investigated; optical losses, cross-sections, lifetimes, and other parameters were measured and calculated from

experimental data [15–20]. Considerable efforts were devoted to numerical simulation of mid-IR chalcogenide fiber lasers; different schemes, including cascade lasing schemes at two successive radiative transitions, were proposed and studied (see book chapter [20] and references therein, as well as original works [16,18,19,21–24]). However, despite the long history of experimental and theoretical works, a fiber laser at a wavelength of about 5 μm based on chalcogenide glasses was first demonstrated only in 2021 [25]. The laser generation with a spike structure at 5.38 μm was achieved in a Tb^{3+} -doped selenide fiber pumped at 1.98 μm [25]. Since then, other chalcogenide fiber lasers have been demonstrated in this spectral range using various rare-earth ions [26,27]. Ce^{3+} -doped laser with mW power, operating near 4.6 μm or near 5 μm (depending on resonator Q-factor), with in-band pump at 4.16 μm was reported in [27]. Currently, to the best of our knowledge, the highest reported power in chalcogenide fiber lasers at wavelengths around 5 μm is 150 mW [26,28].

With the use of single-core chalcogenide glass fibers, the maximum power achieved may be limited by the fiber damage threshold [28]. This limit may be overcome in multichannel systems. However, in multichannel systems with independent channels, it is necessary to provide their coherent combination, which is not an easy task, even in the near-IR range, to say nothing of the mid-IR. In this work, we propose to use a multicore fiber with 25 coupled doped cores arranged in a 5×5 square lattice. At the same time, in such a fiber, the intensity of radiation propagating in each core is reduced, which allows the total power to be increased many times over. When coherently combining channels of multicore fibers, in-phase field distribution is frequently used, which is the most intuitive solution [29,30]. We remind the readers that the in-phase distribution is a wave structure in which the spatial phases of the fields are the same in all cores. However, for the proposed fiber design with coupled cores, we operate with an out-of-phase supermode (in which the spatial phases in the neighboring active cores differ by π) that has a number of advantages compared to the in-phase supermode. As was shown theoretically and experimentally, the in-phase supermode is susceptible to instability at relatively high powers, while the out-of-phase mode is stable [31,32]. Further, the coherent beam combining (CBC) technique for out-of-phase supermode radiation can be easily implemented using only two beam-splitters [33,34]. In this case, a feedback system is not required for channel phasing, and the combining efficiency is significantly higher than that for the in-phase supermode [33]. Moreover, for the out-of-phase supermode, the overlap integral with doped cores is maximal and, hence, the gain is maximal, which makes it possible to implement self-selection of modes in the laser and to obtain lasing in this particular mode. It should be noted that the use of active chalcogenide multicore fibers as a laser medium has not been considered before. The goal of our work is a detailed study of this case, which may be important for the development of mid-IR fiber lasers around 5 μm with a power of several watts.

The rest of the article is organized as follows. In Section 2.1, we describe the laser properties of the considered Tb-doped chalcogenide glass. In Section 2.2, we propose a specific design of a multicore fiber, find the parameters of its out-of-phase supermode in comparison with the in-phase one, and find the efficiency of coherent beam combining of the out-of-phase supermode in the far field. Section 2.3 describes in detail the numerical model used to simulate lasers. Section 3 presents the results of laser modeling and their analysis. Discussion and conclusions are given in Section 4.

2. Materials and Methods

2.1. Model of Active Tb-Doped Chalcogenide Glass

We considered chalcogenide glass doped with Tb ions with a concentration of $2 \times 10^{19} \text{ cm}^{-3}$ as an active medium for lasing, with a focus on the best achievements in the field of synthesis of selenide glasses and the manufacture of optical fibers from them [26]. As far as we know, experimental chalcogenide fiber lasers reported to date were based on selenide glass fibers since they have appropriate optical and physicochemical properties [26]. This is what determined our choice.

Figure 1a shows a simplified diagram of laser levels. We assumed that pumping occurs at a wavelength of about 2 μm at the ${}^7\text{F}_6 \rightarrow {}^7\text{F}_2$ transition, which can be easily achieved using thulium fiber lasers. Moreover, pumping can also be carried out at a slightly shorter wavelength of about 1.9 μm at the ${}^7\text{F}_6 \rightarrow {}^7\text{F}_1$ transition using thulium fiber lasers too [28]. Laser generation can occur at the ${}^7\text{F}_5 \rightarrow {}^7\text{F}_6$ transition at wavelengths of about 5 μm . The emission and absorption cross-sections of this transition are shown in Figure 1b.

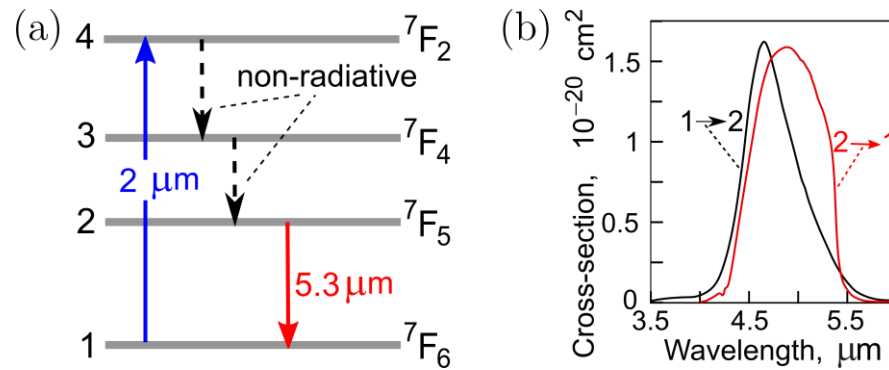


Figure 1. (a) Simplified scheme of the energy levels of Tb³⁺ ions. (b) Emission and absorption cross-sections of ${}^7\text{F}_5 \rightarrow {}^7\text{F}_6$ laser transition.

The parameters of the active Tb-doped Ga–Ge–Sb–Se glass [26,28] used in our simulation are given in Table 1. It is important to note that the lifetime of the upper ${}^7\text{F}_5$ laser level is long enough to create the necessary inversion between this level and the ground state.

Table 1. Tb-doped chalcogenide glass parameters used in modeling (taken from Refs. [20,26,28]).

Parameter	Symbol	Value
Pump wavelength at 1 \rightarrow 4 (${}^7\text{F}_6 \rightarrow {}^7\text{F}_2$) transition	λ_p	2 μm
Laser wavelength at 2 \rightarrow 1 (${}^7\text{F}_5 \rightarrow {}^7\text{F}_6$) transition	λ_s	5.3 μm
Total lifetime of level 2 (${}^7\text{F}_5$)	τ_2	7.5 ms
Total (non-radiative) lifetime of level 3 (${}^7\text{F}_4$)	τ_3	10 μs
Total lifetime of level 4 (${}^7\text{F}_2$)	τ_4	0.1 ms
Absorption cross-section at 1 \rightarrow 4 (${}^7\text{F}_6 \rightarrow {}^7\text{F}_2$) transition	σ_{14}	$0.7 \times 10^{-20} \text{ cm}^2$
Emission cross-section at 4 \rightarrow 1 (${}^7\text{F}_2 \rightarrow {}^7\text{F}_6$) transition	σ_{41}	$0.7 \times 10^{-20} \text{ cm}^2$
Absorption cross-section at 1 \rightarrow 2 (${}^7\text{F}_6 \rightarrow {}^7\text{F}_5$) transition	σ_{12}	$0.35 \times 10^{-20} \text{ cm}^2$
Emission cross-section at 2 \rightarrow 1 (${}^7\text{F}_5 \rightarrow {}^7\text{F}_6$) transition	σ_{21}	$1.09 \times 10^{-20} \text{ cm}^2$

2.2. Model of Multicore Fiber: Features and Advantages of Out-of-Phase Supermode

The cross-section of the considered active selenide fiber is shown in Figure 2a. We proposed a fiber design with 25 cores arranged in a 5×5 square lattice. The diameter of each Tb-doped core was set to 20 μm , and the distance between the centers of neighboring cores was set to 25 μm . The refractive index of the cores was $n \sim 2.545$, which corresponds to a Fresnel reflection coefficient of 19% at a wavelength of 5.3 μm . The refractive index of the undoped cladding was 2.538 (the cladding was assumed to be made of Ga–Ge–Sb–Se selenide glass with slightly different exact composition compared to the glass matrix of the cores). For such a fiber, the V-parameter is 2.236 at a wavelength of 5.3 μm , i.e., each core is single-mode at the laser signal wavelength. The cladding diameter was 300 μm . The diameter and the glass composition of the second cladding (“cladding 2” in Figure 2a) are not important in our model, but its refractive index must be lower than the refractive index of the 300 μm undoped cladding for waveguide propagation of the pump. We calculated the supermodes of such a fiber using the finite element method. The fields of the fundamental in-phase supermode and the higher out-of-phase supermode are shown in Figure 2b,c, respectively. It can be seen that the out-of-phase mode is much better localized near the cores; between the cores, there are lines on which the fields take zero values. For

an in-phase supermode, the fields are notably wider. The effective mode areas A_{eff} are calculated as follows:

$$A_{eff} = \frac{\left(\iint_{-\infty}^{+\infty} P_z dx dy \right)^2}{\iint_{-\infty}^{+\infty} P_z^2 dx dy}, \quad (1)$$

where P_z is the longitudinal z-component of the Poynting vector. We found that A_{eff} is $7017 \mu\text{m}^2$ and $4892 \mu\text{m}^2$ for in-phase and out-of-phase supermodes, respectively. In this case, the overlap integrals of supermodes with doped cores calculated as

$$\Gamma_s = \frac{\iint_{\text{cores}} P_z dx dy}{\iint_{-\infty}^{+\infty} P_z dx dy} \quad (2)$$

which are 0.74 and 0.91 for in-phase and out-of-phase supermodes, respectively.

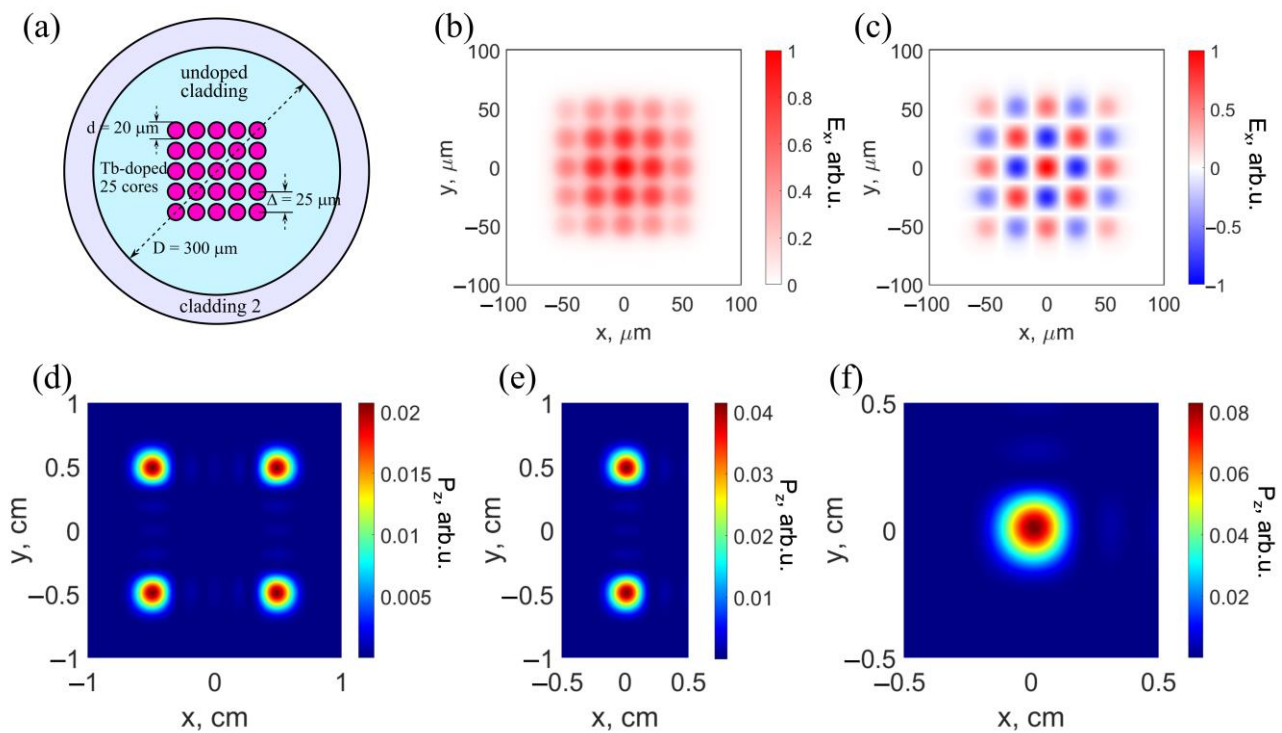


Figure 2. (a) Cross-section of chalcogenide multicore fiber with Tb-doped cores arranged in a 5×5 square lattice. Modeled electric fields of in-phase (b) and out-of-phase (c) supermodes. Intensity distributions of the laser beam before (d), after one (e), and after two (f) steps of CBC, calculated in the far field after propagating a path of 5 cm.

Next, we considered CBC of the out-of-phase supermode in the far field using two beam splitters, described in detail in [33,34]. The far field intensity found after the 2D Fourier transform is shown in Figure 2d. The intensity after combining at the first beamsplitter is shown in Figure 2e and after combining at two beamsplitters in Figure 2f. In this case, the combining efficiency was 98%.

2.3. Modeling Laser Action in Tb-Doped Chalcogenide Multicore Fibers

A simplified laser scheme based on the proposed Tb-doped chalcogenide multicore 5×5 fiber is shown in Figure 3a. We assumed that the reflection coefficient for the signal at the pump end was close to 1. We also assumed that the unabsorbed pump power was not reflected from the output end. The reflection coefficient at the output end R_2 varied for the laser wave. We calculated the output power. Further, by calculating the far field distributions and applying two consecutive steps of coherent combining with

two beamsplitters, we modeled a highly efficient system for coherent beam combining of an out-of-phase supermode, as described in Section 2.2.

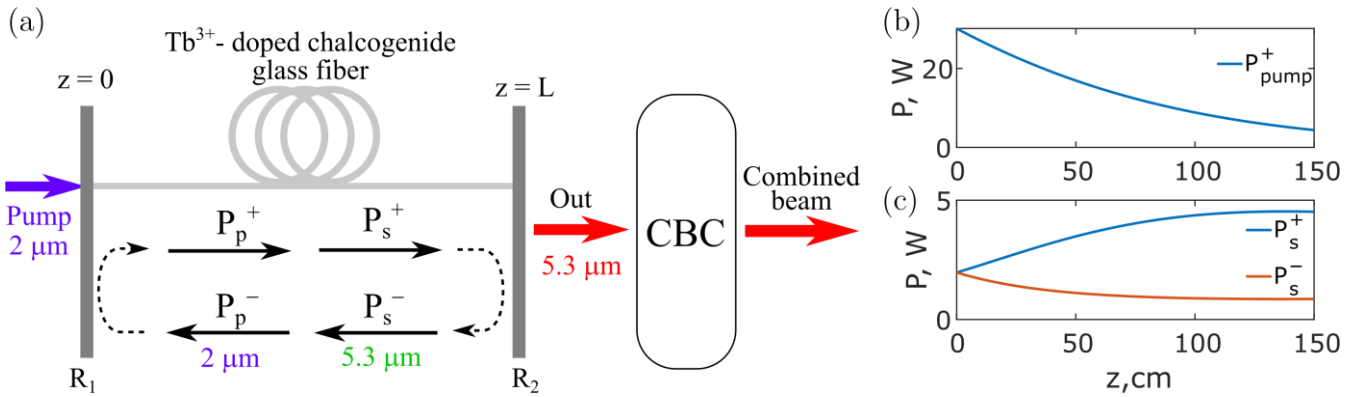


Figure 3. (a) Scheme of Tb-doped chalcogenide glass fiber laser. CBC is the system for coherent beam combining by summing out-of-phase supermode with two beamsplitters. Evolution of intracavity powers at pump wavelength (b) and at signal wavelength (c) modeled for $P_{pump} = 30$ W, $L = 150$ cm, and $R_2 = 0.19$.

To simulate a laser based on a double-clad Tb-doped chalcogenide glass multicore fiber, we implemented a numerical model taking into account rate equations for levels 7F_6 , 7F_5 , 7F_4 , and 7F_2 , equations for the evolution of pump and signal (laser) waves along the z -coordinate, and boundary conditions at the fiber ends. The rate equations for the population densities n_1 , n_2 , n_3 , and n_4 (normalization to the concentration of Tb^{3+} ions in the core $N_{Tb} = 2 \times 10^{-19} \text{ cm}^{-3}$) read [20]

$$\frac{\partial n_1}{\partial t} = -(W_{12} + W_{14})n_1 + \left(W_{21} + \frac{1}{\tau_2}\right)n_2 + W_{41}n_4 = 0 \quad (3)$$

$$\frac{\partial n_2}{\partial t} = W_{12}n_1 - \left(W_{21} + \frac{1}{\tau_2}\right)n_2 + \frac{n_3}{\tau_3} = 0 \quad (4)$$

$$\frac{\partial n_3}{\partial t} = -\frac{n_3}{\tau_3} + \frac{n_4}{\tau_4} = 0 \quad (5)$$

$$n_1 + n_2 + n_3 + n_4 = 1, \quad (6)$$

where t is time; τ_2 , τ_3 and τ_4 are the lifetimes of levels 2 (7F_5), 3 (7F_4), and 4 (7F_2), respectively; and W_{kl} are the stimulated emission (if $k > l$) and absorption (if $k < l$) rates from level k to level l . The stimulated emission and absorption rates for the pump are [20]

$$W_{41,14} = \frac{\Gamma_p \lambda_p \sigma_{41,14} (P_p^+ + P_p^-)}{hcA_c}, \quad (7)$$

where h is Planck's constant, c is the speed of light in vacuum, σ_{kl} are cross sections, λ_p is the pump wavelength, P_p^+ (P_p^-) is the intracavity power at λ_p propagating in the forward (backward) direction (see Figure 3a), $A_c = N \times N \times \pi d^2/4$ is the area of all $N \times N$ Tb-doped cores, and Γ_p is the overlap integral of the pumping wave with all doped cores evaluated as $\Gamma_p = A_c/(\pi D^2/4)$. The stimulated rates for the signal (laser) waves at λ_s are [20]

$$W_{21,12} = \frac{\Gamma_s \lambda_s \sigma_{21,12} (P_s^+ + P_s^-)}{hcA_c}, \quad (8)$$

where Γ_s is the overlap integral defined by Equation (1) and P_s^+ and P_s^- are the intracavity powers of the forward-propagating and backward-propagating laser waves at λ_s .

The equations for the intracavity power evolution are written as [20]

$$\pm \frac{dP_p^\pm}{dz} = \Gamma_p N_{Tb} (\sigma_{41} n_4 - \sigma_{14} n_1) P_p^\pm - \alpha_p P_p^\pm \tag{9}$$

$$\pm \frac{dP_s^\pm}{dz} = \Gamma_s N_{Tb} (\sigma_{21} n_2 - \sigma_{12} n_1) P_s^\pm - \alpha_s P_s^\pm, \tag{10}$$

where α_p and α_s are the background fiber losses at λ_p and λ_s . The boundary conditions for Equations (9) and (10) are [20]

$$P_s^+(0) = R_1 P_s^-(0) \tag{11}$$

$$P_s^-(L) = R_2 P_s^+(L) \tag{12}$$

$$P_p^+(0) = R_1 P_p^-(0) \tag{13}$$

$$P_p^-(L) = R_2 P_p^+(L). \tag{14}$$

The output power P_{out} at 5.3 μm is calculated as

$$P_{out} = P_s^+(L) \times (1 - R_2). \tag{15}$$

All parameters used in modeling are summarized in Tables 1 and 2.

Table 2. Problem parameters used in modeling.

Parameter	Symbol	Value
Cavity multicore fiber length	L	30–300 cm
Diameter of Tb-doped core	d	20 μm
Distance between core centers	Δ	25 μm
Tb concentration in the core	N_{Tb}	$2 \times 10^{-19} \text{ cm}^{-3}$
Numerical aperture (cores/cladding)	NA	0.189
Cladding diameter	D	300 μm
Effective mode field area at $\lambda_s = 5.3 \mu\text{m}$	A_{eff}	4892 μm^2
Overlap integral (pump with Tb-doped cores)	Γ_p	0.11
Overlap integral (laser wave with Tb-doped cores)	Γ_s	0.91
Background fiber loss	α	1.7 dB/m (for Figures 4–8) 0.5–5 dB/m (for Figures 9 and 10)
Reflection coefficient at $z = 0$	R_1	0.999
Reflection coefficient at $z = L$ for laser wave	R_2	0.19–0.99

We numerically modeled the system of Equations (9) and (10), taking into account the boundary conditions (11)–(14). An iterative method based on the Runge–Kutta algorithm was implemented.

3. Results

Using the mathematical model described in detail in Section 2, we performed a theoretical study of high-power mid-IR multicore fiber lasers. From the general theory of lasers, it is known that the lasing thresholds, slope efficiencies, and maximum output powers are influenced by various system parameters, such as cavity length, output reflectance, optical losses, etc. [35]. Therefore, we carried out a detailed theoretical study of the behavior of a laser based on the proposed multicore fiber as dependent on various parameters.

First, we set a high pump power $P_{pump} = 30 \text{ W}$ and modeled the output laser power as a function of two variables: cavity fiber length L and output reflection coefficient R_2 (Figure 4). The output power was calculated for each point in the 500×500 grid of parameters (L, R_2) to ensure precision in plotting the dependence. With increasing reflection coefficient, the optimal length decreased, as shown by the dotted line in Figure 4. Hereinafter, we set the minimum value of output reflectivity $R_2 = 0.19$, which corresponds to the coefficient

of Fresnel reflection from the chalcogenide fiber end [28]. In the simplest case, an increase in the reflection coefficient can be achieved using external mirrors [28]. In principle, there are technologies for applying special coatings to the fiber end, which can either increase or decrease R_2 . But such technologies for chalcogenide glasses are not widespread and well-developed, so, in the analysis, we are limited to $R_2 = 0.19$. It is seen from Figure 4 that the maximum laser powers are achieved precisely at minimum R_2 . Note that the highest laser power in a mid-IR fiber laser based on a single-core chalcogenide fiber was obtained when the fiber end was used as an output reflector [28]. For the multicore fiber considered in Figure 2, it can be seen that the optimal cavity length is 100–150 cm, allowing output powers >3.5 W to be obtained in 25 phased channels at a pump power of 30 W.

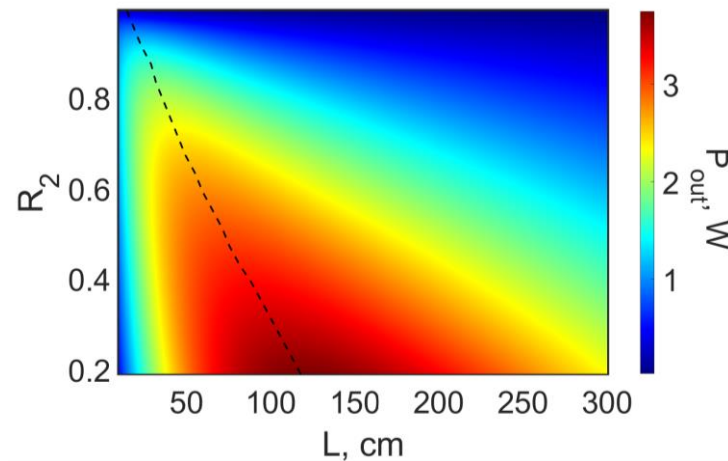


Figure 4. Output laser power vs. fiber cavity length L and reflection coefficient R_2 for $P_{pump} = 30$ W. The dashed curve shows the optimal fiber length that maximizes output laser power for certain R_2 .

Next, we fixed the length of the resonator $L = 150$ cm and plotted the dependence of the output laser power on two variables, which are the pump power P_{pump} and the output reflection coefficient R_2 on the 500×500 grid (Figure 5). In this case, the output power at high reflection coefficients is significantly inferior to the output power at low values of R_2 . This is also explained by the fact that, for large R_2 , the optimal resonator length is significantly less than 150 cm (Figure 4).

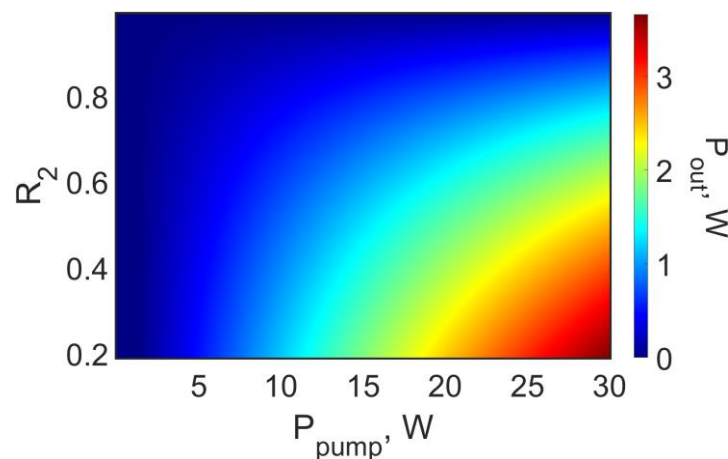


Figure 5. Output laser power vs. pump power P_{pump} and reflection coefficient R_2 for $L = 150$ cm.

Then, we plotted standard dependences of the output power on the pump power at two values of cavity length: $L = 100$ cm (Figure 6a) and $L = 150$ cm (Figure 6b) for different reflectance values. It can be seen that the efficiency is significantly higher for small R_2 . Laser thresholds are visible in enlarged subplots. The larger the value of R_2 , the lower the

threshold, which is fully consistent with the general theory of lasers [35]. The considered resonator lengths differ by a factor of 1.5, but the output powers with the same parameters change slightly for high P_{pump} .

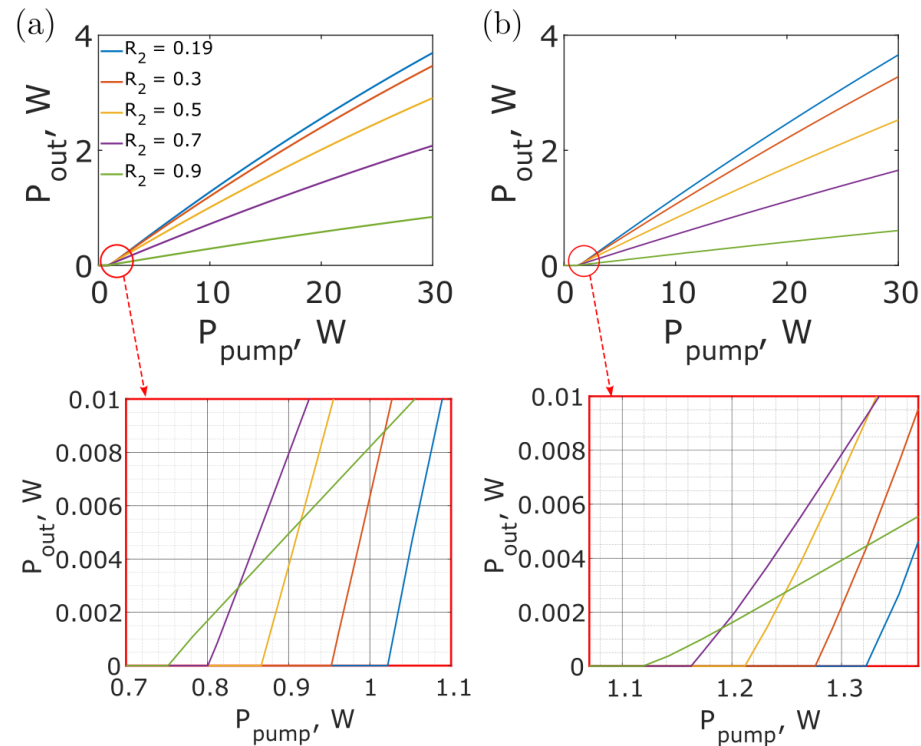


Figure 6. Output laser power vs. pump power, modeled for $L = 100$ cm (a) and $L = 150$ cm (b) and varied R_2 .

Next, we studied in more detail the influence of the cavity length on the output laser power. Figure 7 shows the dependence of the output power on the resonator length and pump power at a fixed optimal value $R_2 = 0.19$ on the 500×500 grid. The dotted line shows the optimal length for a fixed pump power. It can be seen that, the greater the power, the longer this length. At the same time, the optimum is quite smooth, i.e., even with a noticeable deviation from the optimal length, the output power does not change much.

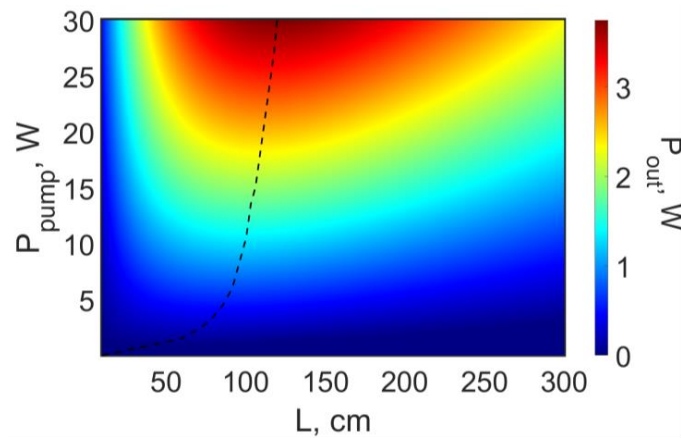


Figure 7. Output laser power vs. fiber cavity length L and pump power P_{pump} for $R_2 = 0.19$. The dashed curve shows the optimal fiber length that maximizes output laser power for certain P_{pump} .

For a better visual perception, we plotted the dependence of the output laser power on the resonator lengths for varying reflection coefficients at three different values of pump

power: $P_{pump} = 10$ W (Figure 8a); $P_{pump} = 20$ W (Figure 8b); and $P_{pump} = 30$ W (Figure 8c). These dependences clearly show that the maxima are quite smooth. At pump powers <10 W, lengths <100 cm should be chosen. But the expected output powers are not very high, so simpler fiber designs are suitable to achieve them.

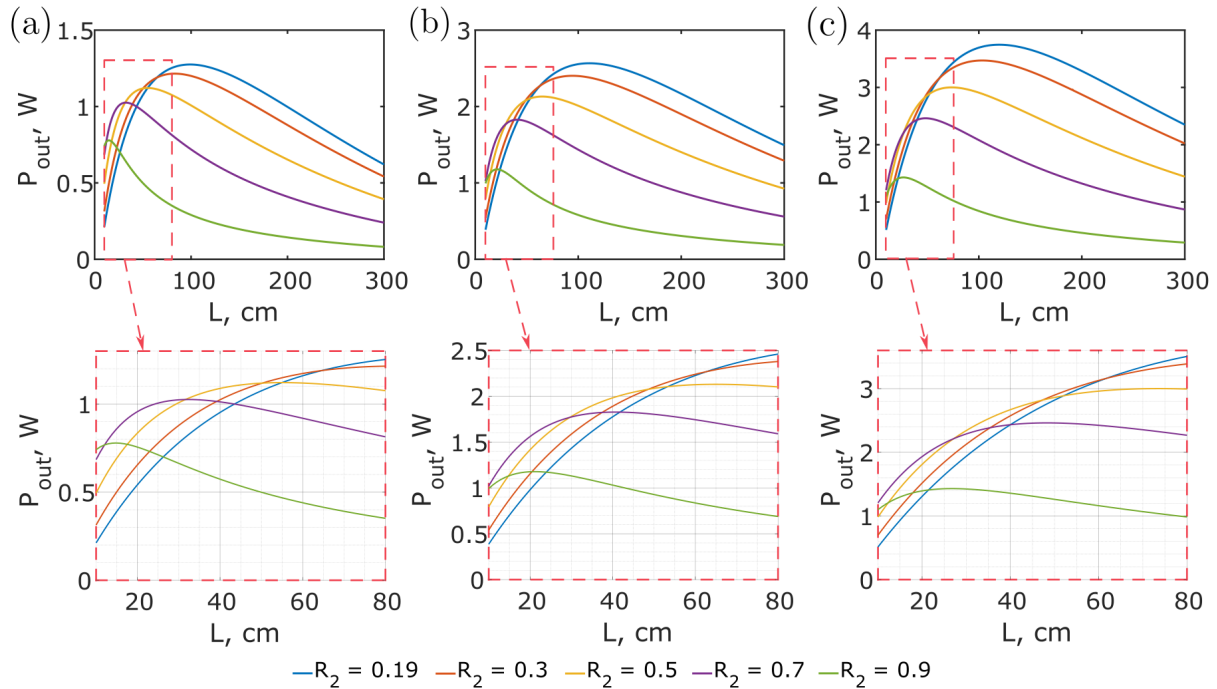


Figure 8. Output laser power vs. fiber intracavity length modeled for $P_{pump} = 10$ W (a); $P_{pump} = 20$ W (b); and $P_{pump} = 30$ W (c) for varied R_2 .

In a series of numerical experiments (see Figures 4–8), we set the value of loss $\alpha = 1.7$ dB/m, as in experimental work [28]. Note that, for different samples of chalcogenide fibers, background losses can be either larger or, in principle, smaller. Therefore, we also investigated the impact of background fiber losses on laser performance. We plotted the expected output power versus pump power for varying losses (Figure 9). The enlarged dependences, where the lasing thresholds are clearly visible, are shown on the right panel. Indeed, losses greatly affect the generation efficiency. It can be seen that, at a loss level of ≤ 1 dB/m, laser powers >5 W are expected to be obtained. At the same time, due to the reduction in heat dissipation during pump thermalization, the influence of parasitic thermo-optical effects is reduced, which is also a favorable factor for the development of a laser system.

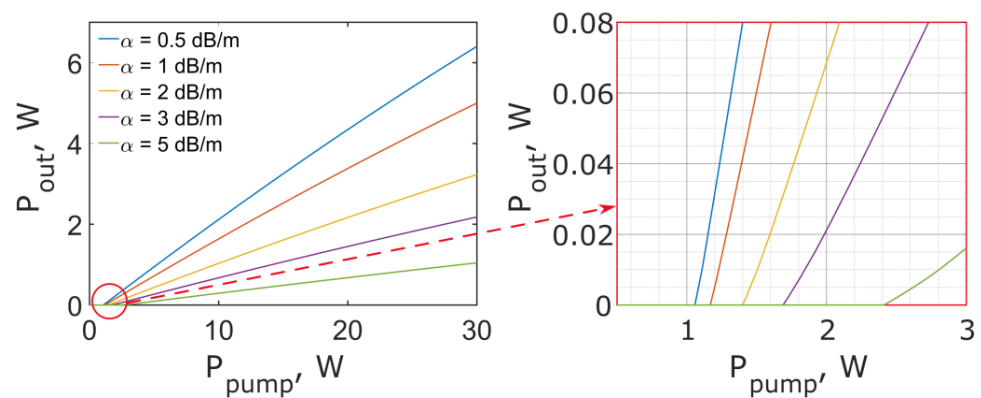


Figure 9. Output laser power vs. pump power, modeled for $L = 150$ cm, $R_2 = 0.19$, and varied fiber background losses.

We plotted the output power as a function of the fiber cavity length for varying losses for a pump level of 30 W (Figure 10a) as well as for a pump level of 100 W (Figure 10b). At the same time, we assumed that the fiber would not be damaged under the action of such high power. Note that, in contrast to the experimental work in [28], where pumping was carried out into a core with a diameter of 19 μm , in our case, we considered pumping into a cladding of a significantly larger diameter of 300 μm (pumping into a cladding is a standard technique for high-power fiber lasers). Therefore, in our case, at $P_{\text{pump}} = 100$ W, the pump intensity is even lower than that achieved in [28]. In this case, the predicted laser powers reach a level of 10 W, which is undoubtedly interesting for many applications (atmosphere monitoring, astronomy, lidars, and so on).

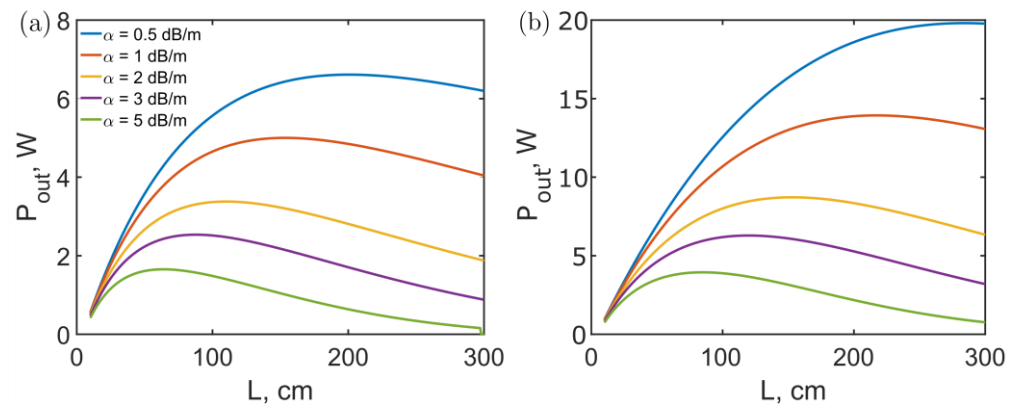


Figure 10. Output laser power vs. fiber intracavity length, modeled for $P_{\text{pump}} = 30$ W (a); $P_{\text{pump}} = 100$ W (b), $R_2 = 0.19$, and varied fiber background losses.

4. Discussion and Conclusions

We have studied in detail a mid-IR chalcogenide multicore fiber laser at a wavelength of 5.3 μm with an output power level of several watts when pumped into the cladding at a wavelength of 2 μm . We proposed to use a Tb-doped chalcogenide multicore fiber with 25 single-mode cores arranged in a 5×5 square lattice as the active medium. This exceeds the power limit of single-core fibers. For the proposed multicore fiber design, the out-of-phase supermode has a significantly larger overlap integral with doped cores than the in-phase supermode. Therefore, the gain for the out-of-phase supermode is maximal, which makes it possible to achieve self-selection of spatial modes and obtain lasing in the out-of-phase mode. If necessary, additional measures for suppression of other modes can be implemented, for example, by inserting a spatial filter between the mirror and the fiber end and placing a mask with four holes that correspond to the locations of the beams (as in Figure 2d) in the Fourier plane of the filter. Moreover, at the output, all channels can be coherently combined, with an efficiency of 98%, using two beamsplitters. Note that this idea of simple, highly efficient coherent beam combining for one-dimensional and two-dimensional beam arrays with out-of-phase spatial distribution of the fields in adjacent channels was experimentally and theoretically demonstrated in [33,34].

When modeling fiber lasers, we specified realistic parameters of Tb-doped chalcogenide glass, focusing on the experimental data in work [28]. We have made a comprehensive theoretical analysis and studied the influence of various factors on the generation parameters. We have shown that a higher lasing efficiency is achieved with the use of Fresnel reflection at the fiber end rather than using an additional mirror that increases the reflection coefficient, which is in excellent agreement with experimental data [28]. We have shown that a laser power of several watts at a wavelength of 5.3 μm can be generated with a pump power of ~ 30 W for an active fiber length of ~ 100 – 150 cm. We have also investigated the effect of background fiber losses and have shown that, when they are reasonably reduced to < 1 dB/m, the output power is expected to increase to > 5 W (with a pump power of 30 W). Moreover, the lower the losses, the lower the parasitic contribution

from thermo-optical effects that arise during pump power thermalization [36–38]. We have also shown that a power level of 10 W in the mid-IR range is theoretically achievable at pump intensities that are experimentally supported by a single-core fiber [28].

Thus, the design of a fiber laser at a wavelength of 5.3 μm based on a Tb-doped chalcogenide multicore fiber proposed in our work may be useful for the development of laser systems with a power level of several watts, which can be interesting for practical applications (atmosphere monitoring, astronomy, lidars, and so on).

Author Contributions: Conceptualization, E.A.A.; methodology, N.I.S. and E.A.A.; software, N.I.S.; validation, N.I.S., A.V.A. and E.A.A.; formal analysis, N.I.S. and E.A.A.; investigation, N.I.S. and E.A.A.; data curation, N.I.S.; writing—original draft preparation, N.I.S. and E.A.A.; writing—review and editing, A.V.A.; visualization, N.I.S. and E.A.A. All authors have read and agreed to the published version of the manuscript.

Funding: This research was funded by the Russian Science Foundation, grant no. 23-12-00248, with the exception of the study of coherent beam combining, the result of which is presented in Figure 2d–f. The study of coherent beam combining was supported by the Center of Excellence’s “Center of Photonics”, funded by the Ministry of Science and Higher Education of the Russian Federation, contract No. 075-15-2022-316.

Data Availability Statement: Data underlying the results presented in this article may be obtained from the authors upon reasonable request.

Conflicts of Interest: The authors declare no conflicts of interest.

References

1. Jackson, S. Towards high-power mid-infrared emission from a fibre laser. *Nat. Photonics* **2012**, *6*, 423–431. [[CrossRef](#)]
2. Ebrahim-Zadeh, M.; Sorokina, I.T. *Mid-Infrared Coherent Sources and Applications*; Springer: Dordrecht, The Netherlands, 2008.
3. Faist, J.; Capasso, F.; Sivco, D.L.; Sirtori, C.; Hutchinson, A.L.; Cho, A.Y. Quantum Cascade Laser. *Science* **1994**, *264*, 553–556. [[CrossRef](#)]
4. Hugi, A.; Villares, G.; Blaser, S.; Liu, H.C.; Faist, J. Mid-Infrared Frequency Comb Based on a Quantum Cascade Laser. *Nature* **2012**, *492*, 229–233. [[CrossRef](#)]
5. Silvestri, C.; Qi, X.; Taimre, T.; Bertling, K.; Rakić, A.D. Frequency Combs in Quantum Cascade Lasers: An Overview of Modeling and Experiments. *APL Photonics* **2023**, *8*, 020902. [[CrossRef](#)]
6. Gladyshev, A.V.; Kosolapov, A.F.; Khudyakov, M.M.; Yatsenko, Y.P.; Kolyadin, A.N.; Krylov, A.A.; Pryamikov, A.D.; Biriukov, A.S.; Likhachev, M.E.; Bufetov, I.A.; et al. 4.4- μm Raman Laser Based on Hollow-Core Silica Fibre. *Quantum Electron.* **2017**, *47*, 491–494. [[CrossRef](#)]
7. Bufetov, I.A.; Kosolapov, A.F.; Pryamikov, A.D.; Gladyshev, A.V.; Kolyadin, A.N.; Krylov, A.A.; Yatsenko, Y.P.; Biriukov, A.S. Revolver Hollow Core Optical Fibers. *Fibers* **2018**, *6*, 39. [[CrossRef](#)]
8. Aghbolagh, F.B.A.; Nampoothiri, V.; Debord, B.; Gerome, F.; Vincetti, L.; Benabid, F.; Rudolph, W. Mid IR Hollow Core Fiber Gas Laser Emitting at 4.6 μm . *Opt. Lett.* **2019**, *44*, 383–386. [[CrossRef](#)]
9. Zhou, Z.; Huang, W.; Cui, Y.; Li, H.; Pei, W.; Li, X.; Li, Z.; Wang, M.; Wang, Z. 3.1 W Mid-Infrared Fiber Laser at 4.16 μm Based on HBr-Filled Hollow-Core Silica Fibers. *Opt. Lett.* **2022**, *47*, 5785–5788. [[CrossRef](#)]
10. Cregan, R.F.; Mangan, B.J.; Knight, J.C.; Birks, T.A.; Russell, P.S.J.; Roberts, P.J.; Allan, D.C. Single-Mode Photonic Band Gap Guidance of Light in Air. *Science* **1999**, *285*, 1537–1539. [[CrossRef](#)] [[PubMed](#)]
11. Falconi, M.C.; Laneve, D.; Prudenzano, F. Advances in Mid-IR Fiber Lasers: Tellurite, Fluoride and Chalcogenide. *Fibers* **2017**, *5*, 23. [[CrossRef](#)]
12. Fortin, V.; Bernier, M.; Bah, S.T.; Vallée, R. 30 W Fluoride Glass All-Fiber Laser at 2.94 μm . *Opt. Lett.* **2015**, *40*, 2882–2885. [[CrossRef](#)] [[PubMed](#)]
13. Fortin, V.; Jobin, F.; Larose, M.; Bernier, M.; Vallée, R. 10-W-Level Monolithic Dysprosium-Doped Fiber Laser at 3.24 μm . *Opt. Lett.* **2019**, *44*, 491–494. [[CrossRef](#)] [[PubMed](#)]
14. Maes, F.; Fortin, V.; Poulain, S.; Poulain, M.; Carrée, J.-Y.; Bernier, M.; Vallée, R. Room-Temperature Fiber Laser at 3.92 μm . *Optica* **2018**, *5*, 761–764. [[CrossRef](#)]
15. Shaw, L.B.; Cole, B.; Thielen, P.A.; Sanghera, J.S.; Aggarwal, I.D. Mid-Wave IR and Long-Wave IR Laser Potential of Rare-Earth Doped Chalcogenide Glass Fiber. *IEEE J. Quantum Electron.* **2001**, *37*, 1127–1137. [[CrossRef](#)]
16. Sójka, Ł.; Tang, Z.; Zhu, H.; Bereś-Pawlik, E.; Furniss, D.; Seddon, A.B.; Benson, T.M.; Sujecki, S. Study of Mid-Infrared Laser Action in Chalcogenide Rare Earth Doped Glass with Dy³⁺, Pr³⁺ and Tb³⁺. *Opt. Mater. Express* **2012**, *2*, 1632–1640. [[CrossRef](#)]
17. Tang, Z.; Furniss, D.; Fay, M.; Sakr, H.; Sójka, Ł.; Neate, N.; Weston, N.; Sujecki, S.; Benson, T.M.; Seddon, A.B. Mid-Infrared Photoluminescence in Small-Core Fiber of Praseodymium-Ion Doped Selenide-Based Chalcogenide Glass. *Opt. Mater. Express* **2015**, *5*, 870. [[CrossRef](#)]

18. Sojka, L.; Tang, Z.; Furniss, D.; Sakr, H.; Fang, Y.; Beres-Pawlik, E.; Benson, T.M.; Seddon, A.B.; Sujecki, S. Mid-Infrared Emission in Tb³⁺-Doped Selenide Glass Fiber. *J. Opt. Soc. Am. B* **2017**, *34*, A70–A79. [[CrossRef](#)]
19. Karaksina, E.V.; Shiryaev, V.S.; Churbanov, M.F.; Anashkina, E.A.; Kotereva, T.V.; Snopatin, G.E. Core-Clad Pr(3+)-Doped Ga(In)-Ge-As-Se-(I) Glass Fibers: Preparation, Investigation, Simulation of Laser Characteristics. *Opt. Mater.* **2017**, *72*, 654–660. [[CrossRef](#)]
20. Sojka, L.; Benson, T.M.; Furniss, D.; Tang, Z.; Sakr, H.; Seddon, A.B.; Sujecki, S. The Modelling of Fibre Lasers for Mid-Infrared Wavelengths. *Recent Trends Comput. Photonics* **2017**, *204*, 39–75. [[CrossRef](#)]
21. Quimby, R.S.; Shaw, L.B.; Sanghera, J.S.; Aggarwal, I.D. Modeling of Cascade Lasing in Dy: Chalcogenide Glass Fiber Laser with Efficient Output at 4.5 μm. *IEEE Photon. Technol. Lett.* **2008**, *20*, 123–125. [[CrossRef](#)]
22. Falconi, M.C.; Palma, G.; Starecki, F.; Nazabal, V.; Troles, J.; Adam, J.-L.; Taccheo, S.; Ferrari, M.; Prudeniano, F. Dysprosium-Doped Chalcogenide Master Oscillator Power Amplifier (MOPA) for Mid-IR Emission. *J. Light. Technol.* **2017**, *35*, 265–273. [[CrossRef](#)]
23. Anashkina, E.A.; Kim, A.V. Numerical Simulation of Ultrashort Mid-IR Pulse Amplification in Praseodymium-Doped Chalcogenide Fibers. *J. Light. Technol.* **2017**, *35*, 5397–5403. [[CrossRef](#)]
24. Xiao, X.; Xu, Y.; Guo, H.; Wang, P.; Cui, X.; Lu, M.; Wang, Y.; Peng, B. Theoretical Modeling of 4.3 μm Mid-Infrared Lasing in Dy³⁺-Doped Chalcogenide Fiber Lasers. *IEEE Photonics J.* **2018**, *10*, 1501011. [[CrossRef](#)]
25. Shiryaev, V.S.; Sukhanov, M.V.; Velmuzhov, A.P.; Karaksina, E.V.; Kotereva, T.V.; Snopatin, G.E.; Denker, B.I.; Galagan, B.I.; Sverchkov, S.E.; Koltashev, V.V.; et al. Core-Clad Terbium Doped Chalcogenide Glass Fiber with Laser Action at 5.38 μm. *J. Non-Cryst. Solids* **2021**, *567*, 120939. [[CrossRef](#)]
26. Denker, B.; Fjodorow, P.; Frolov, M.; Galagan, B.; Koltashev, V.; Plotnichenko, V.; Sukhanov, M.; Sverchkov, S.; Velmuzhov, A. Rare earth doped selenide glasses as laser materials for the 5–6 μm spectral range. *Photonics* **2023**, *10*, 1323. [[CrossRef](#)]
27. Koltashev, V.V.; Frolov, M.P.; Leonov, S.O.; Sverchkov, S.E.; Galagan, B.I.; Korostelin, Y.V.; Skasyrsky, Y.K.; Snopatin, G.E.; Sukhanov, M.V.; Velmuzhov, A.P.; et al. Characteristics of a CW ~5 μm Ce³⁺-Doped Chalcogenide Glass Fiber Laser. *Laser Phys. Lett.* **2023**, *20*, 095801. [[CrossRef](#)]
28. Koltashev, V.V.; Denker, B.I.; Galagan, B.I.; Snopatin, G.E.; Sukhanov, M.V.; Sverchkov, S.E.; Velmuzhov, A.P.; Plotnichenko, V.G. 150 mW Tb³⁺ Doped Chalcogenide Glass Fiber Laser Emitting at λ > 5 μm. *Opt. Laser Technol.* **2023**, *161*, 109233. [[CrossRef](#)]
29. Klenke, A.; Müller, M.; Stark, H.; Stutzki, F.; Hupel, C.; Schreiber, T.; Tünnermann, A.; Limpert, J. Coherently Combined 16-Channel Multicore Fiber Laser System. *Opt. Lett.* **2018**, *43*, 1519–1522. [[CrossRef](#)]
30. Fsaifes, I.; Ranély-Vergé-Dépré, C.-A.; Veinhard, M.; Bellanger, S.; Chanteloup, J.-C. Far Field Energy Distribution Control Using a Coherent Beam Combining Femtosecond Digital Laser. *Opt. Express* **2023**, *31*, 8217–8225. [[CrossRef](#)]
31. Balakin, A.A.; Skobelev, S.A.; Andrianov, A.V.; Anashkina, E.A.; Litvak, A.G. Coherent Amplification of High-Power Laser Radiation in Multicore Fibers from a Rectangular Array of Cores. *Opt. Lett.* **2021**, *46*, 246–249. [[CrossRef](#)]
32. Andrianov, A.V.; Kalinin, N.A.; Anashkina, E.A.; Egorova, O.N.; Lipatov, D.S.; Kim, A.V.; Semjonov, S.L.; Litvak, A.G. Selective Excitation and Amplification of Peak-Power-Scalable Out-of-Phase Supermode in Yb-Doped Multicore Fiber. *J. Light. Technol.* **2020**, *38*, 2464–2470. [[CrossRef](#)]
33. Andrianov, A.; Kalinin, N.; Anashkina, E.; Leuchs, G. Highly Efficient Coherent Beam Combining of Tiled Aperture Arrays Using Out-of-Phase Pattern. *Opt. Lett.* **2020**, *45*, 4774–4777. [[CrossRef](#)] [[PubMed](#)]
34. Kalinin, N.A.; Anashkina, E.A.; Leuchs, G.; Andrianov, A.V. Lenslet Array-Free Efficient Coherent Combining of Broadband Pulses at the Output of a Multicore Fiber with a Square Core Grid. *Opt. Express* **2022**, *30*, 1013–1020. [[CrossRef](#)] [[PubMed](#)]
35. Svelto, O.; Hanna, D.C. *Principles of Lasers*; Springer: New York, NY, USA, 2010.
36. Brown, D.C.; Hoffman, H.J. Thermal, Stress, and Thermo-Optic Effects in High Average Power Double-Clad Silica Fiber Lasers. *IEEE J. Quantum Electron.* **2001**, *37*, 207–217. [[CrossRef](#)]
37. Antipov, O.; Dobrynin, A.; Getmanovskiy, Y.; Karaksina, E.; Shiryaev, V.; Sukhanov, M.; Kotereva, T. Thermal Lensing and Laser-Induced Damage in Special Pure Chalcogenide Ge₃₅As₁₀S₅₅ and Ge₂₀As₂₂Se₅₈ Glasses under Quasi-CW Fiber Laser Irradiation at 1908 nm. *Photonics* **2023**, *10*, 252. [[CrossRef](#)]
38. Kuznetsov, I.; Chizhov, S.; Palashov, O. High-Energy and High-Average-Power Two-Channel Yb:YAG Amplifier with Passive Coherent Combining. *J. Opt. Soc. Am. B* **2022**, *39*, 2692–2696. [[CrossRef](#)]

Disclaimer/Publisher’s Note: The statements, opinions and data contained in all publications are solely those of the individual author(s) and contributor(s) and not of MDPI and/or the editor(s). MDPI and/or the editor(s) disclaim responsibility for any injury to people or property resulting from any ideas, methods, instructions or products referred to in the content.